ARTICLE OPEN

Check for updates

Molecular dynamic study of radiation-moisture aging effects on the interface properties of nano-silica/silicone rubber composites

Weitao Lou[1], Chaoyang Xie[2]✉ and Xuefei Guan[1]✉

The influence of radiation-moisture aging on the thermodynamic and interface properties of nano-silica/silicone rubber (PDMS) composites was investigated using molecular dynamics simulation. The deterioration of polymer matrix was incorporated into the PDMS-silica interface models based on the hydrolysis products and the dominant role of cross-linking over chain scission. The results indicate that the long-chain structure with the higher molecular weight and the stronger intermolecular interactions are formed by incorporating multi-chain cross-linking and more hydroxyl groups. The coupling effects of the long-chain structure and stronger intermolecular interactions enhance the binding strength between the silica and PDMS matrix owing to the formation of more hydrogen bonds, and restrict the diffusion mobility of PDMS chains and water molecules. The aging of the PDMS matrix facilitates water molecules to adsorb on the surface of the silica and the PDMS matrix to form hydrogen bonds, and eventually weakens the bonding strength of the silica-PDMS interface.

npj Materials Degradation (2023)7:32 ; https://doi.org/10.1038/s41529-023-00351-8

INTRODUCTION

Silica reinforced silicone rubber composites are made up of polydimethylsiloxane (PDMS), surface-modified silica fillers, and other additives, exhibiting outstanding thermal stability, chemical resistance, and superior elastic recovery property[1–3]. Therefore, silicone rubber composites are often used as insulation, sealing, and cushion materials in power generation, aerospace, and aviation sectors, etc. However, silicone rubber composites inevitably degrade with time, slowly but steadily, during long-term service due to harsh environmental factors such as radiation, moisture, and heat[4–6]. In general, common causes for polymeric composite degradation arise from the absorption of H_2O molecules or radiation during long-term storage[7]. Exposure to hazardous radiation such as gamma radiation can result in chain scission, cross-linking, and the formation of free radicals and gaseous products[8,9]. The moisture can cause hydrolysis of the main chain and side groups accompanied by the formation of hydroxyl groups[10]. The physical and chemical reaction mechanisms may become more complicated in radiation-moisture environments, leading to the deterioration in the long-term performance and service life of the polymeric components. Therefore, understanding the radiolysis mechanism and hydrolysis behaviors of silicone rubber composites has enormous practical applications, ranging from evaluating environmental impacts to constructing aging models for structure-property relationships and the lifetime prediction of silicone rubber components.

During long-term service, the performance degradation of composite material depends on a combined effect of the physical and chemical changes of polymer matrix and fillers[11–13]. Chemical degradation of the PDMS matrix induced by radiation-moisture aging can greatly alter the rubber network structure through cross-linking, chain scission, hydrolysis of the main chain and methyl group, rearrangement, and breakage of side groups[14,15]. Additionally, the surface chemical structure of the nano-silica would change once exposed to radiation and moisture including hydrolysis, breakage, and covalent grafting of surface groups[15–17]. All of these reactions can adversely affect molecular mobility, dispersibility of the filler, and polymer-filler interfacial interactions (e.g., electrostatic force, molecular diffusion, mechanical coupling, chemical bonding, and intermolecular force) which play a crucial role in dominating the properties of the silicone rubber composites[18,19]. For example, the introduction of polar groups during the aging process may enhance the polarity of PDMS, which can improve the interfacial adhesion strength and filler dispersion. The changes in the interfacial adhesion strength and filler dispersion may result in irreversible degradation of the mechanical and thermal properties of the silicone rubber composites. In addition, the deterioration of the PDMS matrix and polymer-filler interface structure can also strongly affect the diffusion of small molecules (e.g., oxygen, H_2O, and free radicals) during the aging process[20,21], which in turn influences radiolysis and hydrolysis reactions. However, the effects of radiation-moisture aging on the interface properties and gas diffusion in silicone rubber composites are less concerned.

Many recent efforts focused on the aging behavior and mechanism of PDMS composites exposed to heat, radiation, atmosphere, and mechanical stress, particularly for radiation and moisture, by a wide range of experiments and modeling approaches[22–26]. The aging-induced physical phenomena and chemical reactions are generally interpreted at different scales. For example, Qin[7] and Wang et al.[27] revealed the influence of gamma irradiation and absorbed moisture on the properties and mechanisms of silicone rubber composites. They found that the absorbed moisture is a key factor during the synergistic aging process. Maiti[28] and Fang et al.[29] developed the radiation age-aware constitutive models of filled silicone elastomer by incorporating the radiation-induced matrix network evolution, which can describe the experimental results well, respectively.

[1]Graduate School of China Academy of Engineering Physics, 100193 Beijing, China. [2]Institute of Systems Engineering, China Academy of Engineering Physics, Mianyang 621900, China. ✉email: xiezy@caep.cn; xfguan@gscaep.ac.cn

Nevertheless, most experimental methods are comparatively difficult to directly detect and quantify the complex polymer network evolution induced by radiation and moisture aging. MD simulation has been increasingly used as an effective tool for investigating the structure-property relationships of polymer composites from the molecular level[30–34], and shows a great promise in revealing the effects of the aging-induced network evolution on the interface properties of silicone rubber composites. Kroonblawd et al.[35,36] proposed a general conditional probability and correlation analysis approach to quantify the causal connections between radiation-induced damage to PDMS through quantum-based molecular dynamics (QMD) simulations. Liu et al.[37] investigated radiolysis mechanisms and structure deterioration of PDMS composites through experiments and reactive molecular dynamics (ReaxFF MD) simulations. They found that radiation-induced radicals are critical for the formation of gas products and cross-linking structures, especially for the radical coupling reactions. Thus, MD simulation combined with experimental observables is conducive to better quantitatively understanding the effect of radiation-moisture aging induced network evolution on interface interactions between nano-silica and PDMS matrix at the atomic level during the aging process.

The purpose of this study is to explore the effect of radiation-moisture aging induced structure chemical changes on the thermodynamic and interface properties of nano-silica/PDMS composites through MD simulation. The aged nano-silica/PDMS and PDMS-silica interface models with or without H_2O molecules were constructed by incorporating the hydrolysis products, cross-linking, and chain scission. The competition between cross-linking and chain scission was also considered in the constructed molecular models. The structure, thermodynamic, and interface properties were evaluated by obtaining the density, mean square displacement (MSD), diffusion coefficients, free accessible volume, hydrogen bonds, relative concentration, and radial distribution function (RDF). The diffusion behaviors of H_2O molecules in the nano-silica/PDMS matrix and the interface between the PDMS matrix and silica layer were estimated by MSD, diffusion coefficients, diffusion trajectory, and hydrogen bonds. All the investigations were performed based on all-atom MD.

RESULTS AND DISCUSSION

Effect of aging on structure and dynamics properties of nano-silica/PDMS composites

The structure and dynamics properties of silica reinforced silicone rubber composites are closely related to the microstructure changes induced by radiation-moisture aging. Here the density, mean square displacement (MSD), diffusion coefficients, fractional accessible volume (FAV), and hydrogen bonds (H-bonds) of systems were obtained based on the results after the product run. For each nano-silica/PDMS system, a relatively small fluctuation (1-2%) for the simulated density is observed during 1000 ps NPT (constant number of particles, pressure, and temperature) simulation at 298 K and 1 atm. The average density of the unaged nano-silica/PDMS system (Model 1) is about 1.068 g cm^{-3}, which is consistent with the experimental values already reported (1.02–1.4 g cm^{-3}) depending on the content of nano-silica and material processing[38]. The result verifies the reliability of the nano-silica/PDMS model. Furthermore, the average densities of Model 2, Model 3, and Model 4 are 1.088 g cm^{-3}, 1.094 g cm^{-3}, and 1.102 g cm^{-3}, respectively, implying that the aging of the PDMS matrix induces the increase of the density.

To quantify the effect of radiation-moisture aging on the dynamic properties of nano-silica/PDMS, the MSD and self-diffusion coefficient (D_s) were calculated to evaluate the mobility and diffusion property of PDMS chains, as follows:[39]

$$\mathrm{MSD} = \left\langle |r_i(t) - r_i(0)|^2 \right\rangle \tag{1}$$

$$D_S = \frac{1}{6N} \lim_{t\to\infty} \frac{d}{dt} \sum_{i=1}^{N} \left\langle |r_i(t) - r_i(0)|^2 \right\rangle \tag{2}$$

where $r_i(0)$ is the initial position coordinate of atom i, and $r_i(t)$ is the position coordinate of atom i at time t, and N is the number of atoms in the selected molecule. Figures 1 and 2 show the MSD and D_s of the main chain, oxygen of the hydroxyl group, cross-link point, and the typical structure in the unaged and aged nano-silica/PDMS systems, respectively. It can be found that the MSD and D_s of the main chain in Model 2, Model 3, and Model 4 systems exhibit smaller values than that of the Model 1 system, implying that the aging of the PDMS matrix lowers the mobility of the main chain. In addition, the order of the D_s of the main chain in different aged nano-silica/PDMS systems is Model 2 > Model 3 > Model 4, indicating that the mobility of the main chain gradually decreases with the increase in the aging level of the PDMS matrix. It can be seen from Figs. 1(b) and 2 that the MSD and D_s of the oxygen of the hydroxyl group are noticeably higher than that of the main chain in the same systems, due to the stronger mobility of side and end groups. Moreover, the higher the aging level of the PDMS matrix, the lower the mobility of the oxygen of the hydroxyl group.

Generally, radiation-moisture aging-induced chemical changes of the PDMS matrix can result in changes in molecular structure, intermolecular interactions, and free volume, which can either promote or inhibit chain mobility. The MSDs of typical cross-linking and chain scission are also obtained, as shown in Fig. 1c, d). The results show that the MSD and D_s of the cross-linking point are less than that of the main chain, indicating that the formation of cross-linking structure seriously limits the diffusion of PDMS chains owing to the long chain structure. In particular, three and four-chain crosslinking structures with higher molecular weights show lower molecular mobility. Furthermore, the MSD of chain scission in Model 3 is larger than that of the main chain and cross-linking structure in Model 3 and Model 4, which reveals that the formation of short chains induced by chain scission improves molecular mobility. However, the dominant role of cross-linking has a more important effect on chain mobility than chain scission.

The intermolecular interactions also play a key role in the structure and dynamic properties of nano-silica/PDMS systems, especially for the strong polar interaction in systems, which can further restrict the movement of molecules. During the aging process, radiation and moisture-induced hydrolysis of the main chains and side groups produces more hydroxyl groups, which contributes to the strengthening of the strong polar interaction such as electrostatic, Van der Waals (vdW), and hydrogen bonds (H-bonds) interactions. The type and number of H-bonds in the different nano-silica/PDMS systems were analyzed and calculated, as shown in Figs. 3 and 4. In this study, two molecules are chosen as being hydrogen only if their inter-oxygen distance is less than 2.7 Å, and simultaneously the O-H…O angle is more than 90°[40,41]. The results show that two types of H-bonds exist in the unaged and aged nano-silica/PDMS systems. The interactions between hydroxyl groups (the surface of nano-silica and the side group of PDMS) and the hydroxyl groups (the surface of nano-silica and the side group of PDMS) form the type A -O-H…O H-bond. The type B -O-H…O H-bond is formed between the hydroxyl groups (the surface of nano-silica and the side group of PDMS) and the oxygen from the Si-O-Si main chain (PDMS). Additionally, the total number of H-bonds conforms to an order: Model 3 > Model 2 > Model 4 > Model 1. This demonstrates that the introduction of more hydroxyl groups induced by hydrolysis increases the probability for H-bonds to form. However, the formation of three and four-chain cross-linking structures lower the probability for the

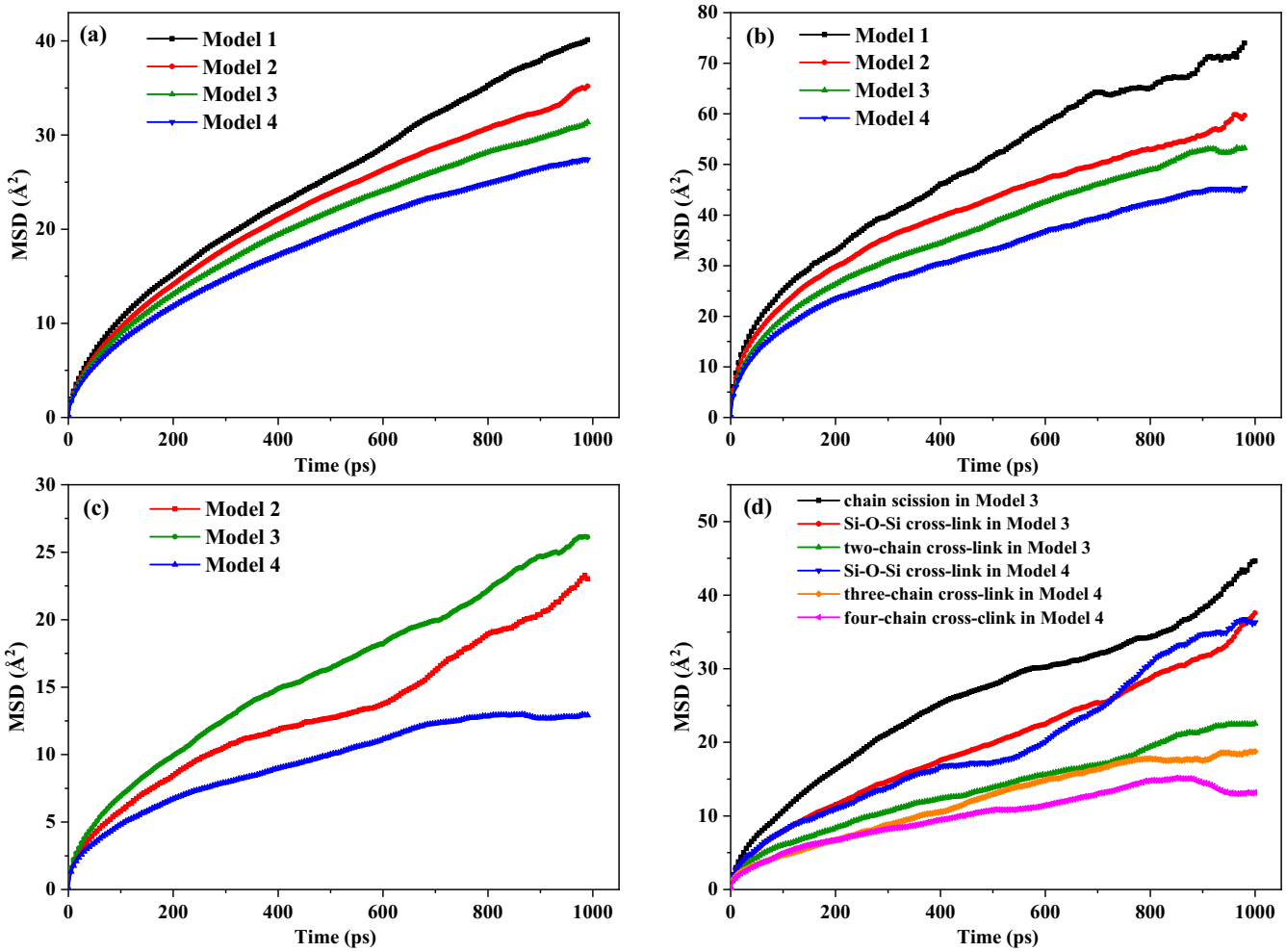

Fig. 1 MSDs of the unaged and aged nano-silica/PDMS models as a function of simulation time. a Main chain of PDMS, **b** oxygen of hydroxyl group of PDMS chain, **c** cross-link point in PDMS matrix, and **d** typical structure in PDMS matrix.

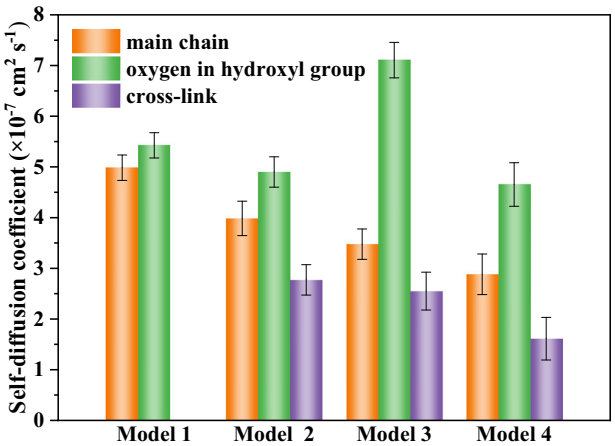

Fig. 2 Self-diffusion coefficients of the main chain, oxygen of hydroxyl group, and cross-link point in the unaged and aged nano-silica/PDMS models. The error bars stand for the standard deviations from five independent sample.

formation of H-bond$_A$ by constraint the movement of the hydroxyl groups, which agrees well with the results of MSD of hydroxyl groups in Model 4 system (Fig. 1b). For the aged nano-silica/PDMS systems, the denser molecular structure induced by multi-chain cross-linking is conducive to the formation of H-bond$_B$ by facilitating the interaction between hydroxyl groups and main chains. Moreover, the large amount of H-bonds at the interface region enhances the adhesion strength between nano-silica and PDMS chains.

The fractional free volume of polymer can be defined as the ratio of the free volume filled with cavity regions to the total volume of polymer composites, which plays an important effect in the permeation behavior of small molecules. To estimate the effect of radiation-moisture aging on the permeation of H_2O molecules, the fractional accessible volume (FAV) is defined as the ratio of the free volume where the water molecule can permeate to the total volume of polymer composites[42,43]. The FAV is quantitatively assessed by a probing spherical particle with a radius equivalent to the vdW radius of H_2O molecules (1.583 Å)[44] to measure whether a volume can be accessible. Figure 5 shows the temperature dependence of FAVs of the nano-silica/PDMS systems with different aging levels for H_2O molecules. As can be observed, the FAVs of the different nano-silica/PDMS systems increase continuously with an increase in temperature, which proves that the increase in temperature increases the accessible volume and promotes the permeation ability of H_2O molecules. Additionally, the unaged nano-silica/PDMS system (Model 1) exhibits a larger FAV for H_2O molecules than that of the aged nano-silica/PDMS systems for H_2O molecules, which means that the polymer aging results in a weaker chain stacking and reduces the accessible volume. Meanwhile, the FAVs for H_2O molecules

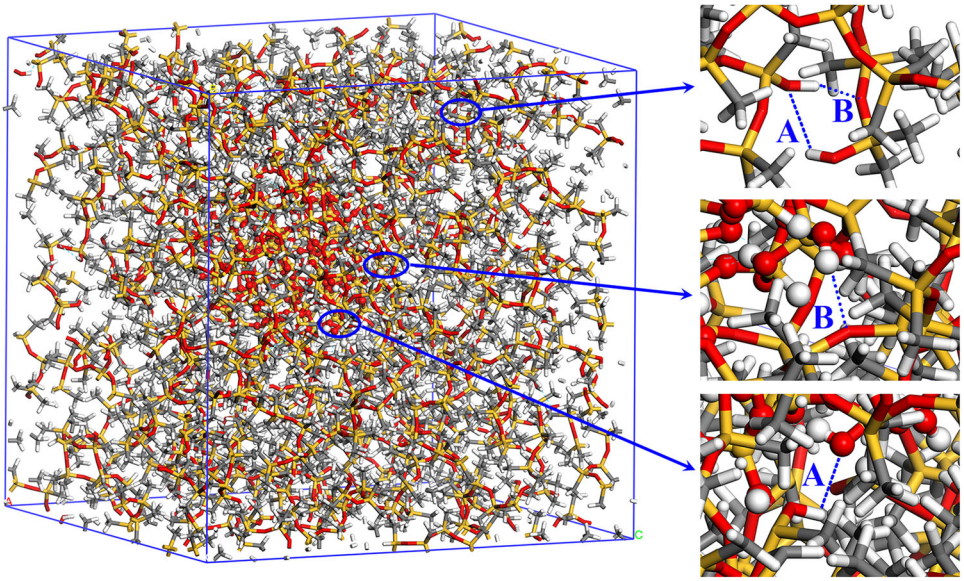

Fig. 3 The types of H-bonds in the Model 3 system.

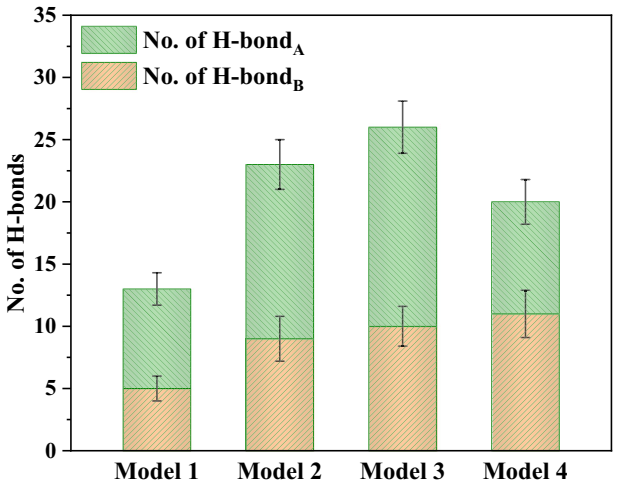

Fig. 4 The number of H-bonds in the different nano-silica/PDMS systems. The error bars stand for the standard deviations from five independent sample.

gradually increase with an increase in the aging level, implying that the introduction of more hydroxyl groups and cross-links leads to the reduction of accessible volume and inhibits the permeation ability of H_2O molecules. The reason for the aged nano-silica/PDMS systems with lower FAV is because the stronger intermolecular interactions occur between PDMS chains, and nano-silica and PDMS chains, and the formation of the cross-linking structure promotes the aggregation of polymer chains to form the denser PDMS matrix.

Effect of aging on interface properties of silica/PDMS composite

To investigate the effect of radiation-moisture aging on interfacial bonding properties of silica/PDMS composite, the MSDs of PDMS chains at different distances along the Z-direction of the silica-PDMS interface were calculated based on the different silica/PDMS interface model systems, as shown in Fig. 6. It is obvious that the MSDs of the PDMS chains for the unaged and aged interface models increase with an increase in distance, which indicates that the interfacial interactions are gradually weakened with the increase in distance. The strongest interfacial interactions (non-bonded and H-bonds interactions) occur within the range 0–2 Å at the interface, which means the lowest mobility of polymer chains. Moreover, compared with the interface Model 1 system, an obvious decrease in MSD can be observed in the interface Model 4 system at the same distance, which is attributed to the coupling effects of hydroxyl groups and cross-linking structure. On the one hand, the cross-linking structure gives rise to the packing of polymer chains and the decrease in the mobility of main chains near the cross-linked points, facilitating the formation of stronger interfacial interactions between silica and the denser PDMS matrix. On the other hand, the introduction of hydroxyl groups enhances the interfacial interactions via stronger polar interactions. As the aging level increases, the formation of more hydroxyl groups in polymer chains exhibits a higher probability to form stronger polar interactions at the interface.

In addition, the polar interactions at the interface were further analyzed by obtaining the concentration profiles of the hydroxyl groups in the Z-direction of the silica-PDMS interface and the RDF of oxygen atoms (O-O) between the hydroxyl groups of silica and hydroxyl groups of PDMS matrix in different interface model systems, as shown in Figs. 7 and 8, respectively. The RDF is defined as the probability of finding other atoms around the center atoms[45]. It can be seen from Fig. 7 that the hydroxyl groups are highly dispersed and mainly concentrated near the interface region of silica/PDMS. Meanwhile, the peak intensity around 11.1–16.8 Å gradually increases with an increase in aging level, due to the formation and concentration of the more hydroxyl groups induced by radiation-moisture aging. Especially for the interface Model 4 system, the introduction of the multi-chain cross-linking structure significantly intensifies the aggregation of the hydroxyl groups near the surface of the PDMS layer at the interface. The highest peaks of the unaged silica-PDMS interface systems to shift a smaller distance towards the surface of the PDMS layer indicate that the introduction of the cross-links restricts the movement of the hydroxyl groups to the surface of the silica. Generally, the probability of the hydrogen bond formation strongly depends on the concentration of the hydroxyl groups and the distance between the polar groups at the interface.

The results of RDFs show that an obvious peak is observed around 2.5–3.1 Å at the interface of the different silica/PDMS

interface model systems, indicating that hydrogen bonds exist in all systems[46]. However, the interface Model 2 and 3 systems show a higher peak around 2.5–3.1 Å than that of the interface Model 1 and 4 systems, which means the greater probability of the hydrogen bond forming at the interface of the interface Model 2 and 3 systems. Furthermore, the lower peak around 2.5–3.1 Å at the interface of the interface Model 4 system indicates that the formation of the multi-chain cross-linking structure restrains the formation of the hydrogen bonds. These results demonstrate that the multi-chain cross-linked points weaken the hydrogen bonding interactions, but enhance the interfacial interactions including electrostatic and vdW interactions.

Diffusion of H_2O in nano-silica/PDMS and silica-PDMS interface composites

The influence of radiation-moisture aging on the diffusion behaviors of H_2O molecules in the unaged and aged nano-silica/PDMS and silica-PDMS interface were systematically investigated by analyzing MSD, diffusion coefficients, diffusion trajectory, and H-bonds. Figure 9(a) shows the MSDs of H_2O molecules in the unaged and aged nano-silica/PDMS systems at 298 K and 340 K as a function of simulation time. The results show that the MSDs of H_2O molecules in the nano-silica/PDMS systems are in the order: Model 1 > Model 2 > Model 3 > Model 4, which demonstrates that the increase in the aging level of the PDMS matrix gradually lowers the mobility of H_2O molecules. Meanwhile, the diffusion coefficients of H_2O molecules at 298 K and 340 K in the unaged and aged nano-silica/PDMS systems were also evaluated, as shown in Fig. 9b. It is found that the diffusion coefficient of H_2O molecules in the unaged nano-silica/PDMS system at 298 K is 1.32×10^{-5} cm^2 s^{-1}, closer to the earlier reported studies (1.45×10^{-5} cm^2 s^{-1})[47,48]. The result verifies that the diffusion coefficient values of H_2O molecules obtained in this study are reliable and can be applied for qualitative comparison. It is also observed that the MSDs and diffusion coefficients of H_2O molecules in all nano-silica/PDMS systems increase with an increase in temperature. This result is because the increase in temperature also raises the flexibility of PDMS chains and weakens the intermolecular interactions between molecules, which increases the free volume and the number of large channels to make H_2O molecules easier to pass. Thus, the higher temperature enhances the effective thermal movement and diffusion rate of H_2O molecules. However, as the aging level increases, the decrease in diffusion coefficients of H_2O molecules at the same temperature indicates that the aging lowers the diffusion rate of H_2O molecules in the nano-silica/PDMS system. It is because the introduction of more hydroxyl groups and multi-chain cross-linking structures leads to the formation of stronger polar interactions among H_2O molecules, PDMS chain, and nano-silica (Fig. 10a, b), and restricts the thermal motion of polymer chains and H_2O molecules, which reduces the FAV and the number of large channels in a polymer matrix (Fig. 10c–f). Thus, there is a lower probability to obtain continuous and effective thermal movement, which in turn suppresses the hydrolysis reactions to some extent. These phenomena are consistent with the simulation results of FAV (Fig. 5).

To gain further understanding, the typical diffusion trajectories of H_2O molecules in the unaged and aged nano-silica/PDMS systems were extracted to track the movement of H_2O molecules, as shown in Fig. 11. Additionally, the jump times and average cageing time of H_2O molecules in different nano-silica/PDMS models were calculated to investigate the motion models of H_2O molecules, as shown in Fig. 12. It is noted that H_2O molecules

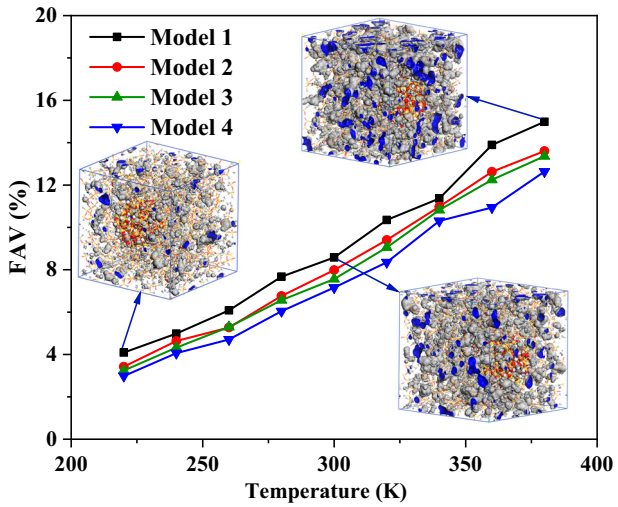

Fig. 5 The temperature dependence of FAVs for H_2O molecules in the unaged and aged nano-silica/PDMS systems. The blue and gray regions in the insets represent the accessible volume and the occupied volume, respectively.

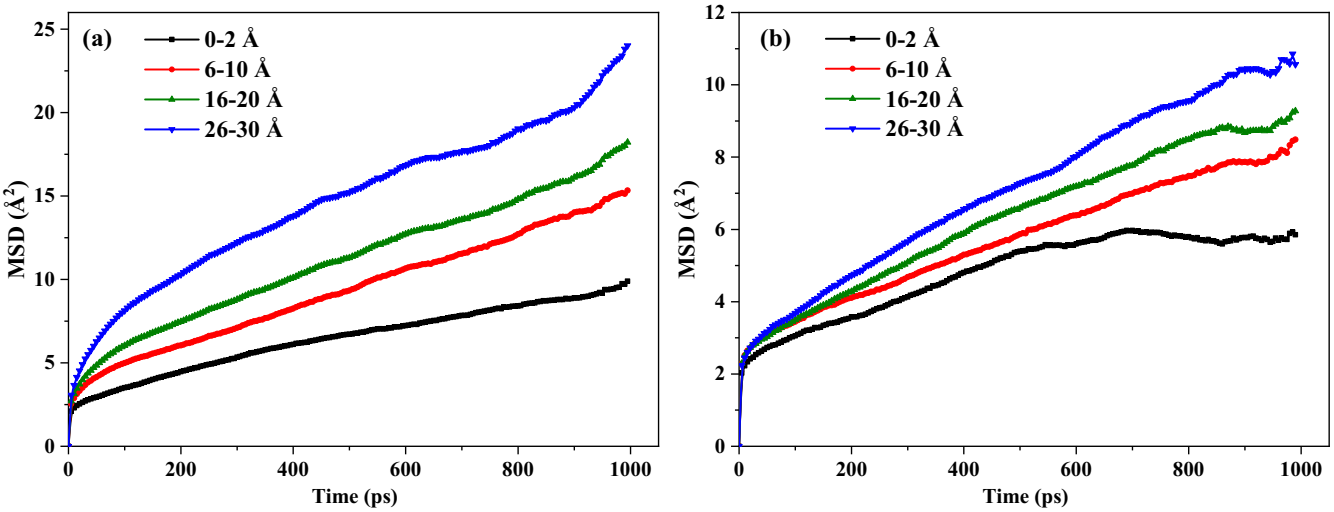

Fig. 6 MSDs of PDMS chains at different distances along the Z-direction of the silica-PDMS interface in different models as a function of simulation time. a the interface Model 1 system, and **b** the interface Model 4 system.

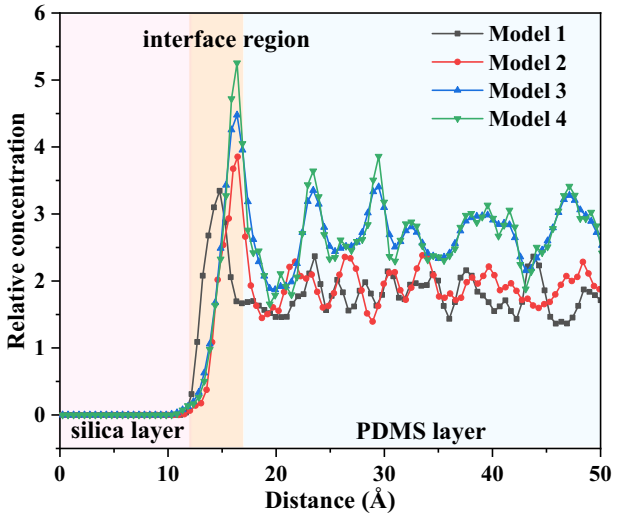

Fig. 7 The relative concentration distributions of the hydroxyl groups in the Z-direction of the silica-PDMS interface in the different interface model systems.

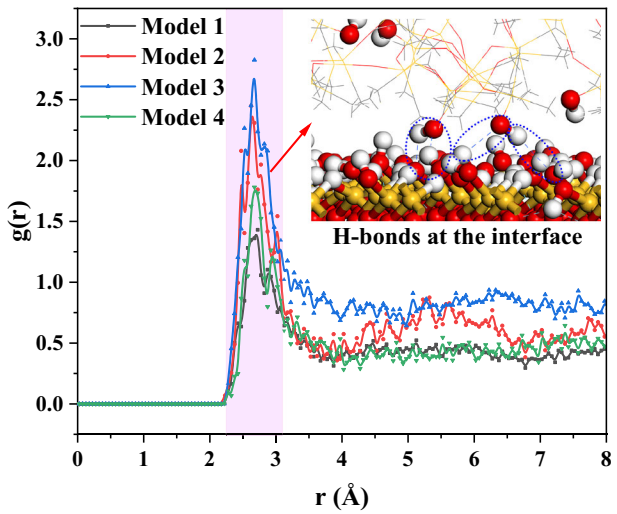

Fig. 8 The RDFs of oxygen atoms (O-O) between the hydroxyl groups of silica and hydroxyl groups of PDMS matrix in the different interface model systems.

permeate in the nano-silica/PDMS by distinct jump-like movements[49]. A representative jump-like event consists of two different models of motion:[50–52] (1) H_2O molecules usually perform a high-frequency vibration in the separated cavities over a relatively long time, and (2) H_2O molecules quickly jump from one cavity to a neighboring cavity by the temporary channels between adjacent cavities formed and destroyed by the thermal motion of PDMS chains. Thus, the diffusion of H_2O molecules happens through a sequence of jumps. According to the diffusion displacements of H_2O molecules, it can be found that the lengths of the oscillating motions are less than 4 Å, whereas the lengths of the jumps are of the order of 4-9 Å. The total timeframe for the execution of a molecular jump is about 5 ps (5×10^{-12} s).

Figures 11 and 12 show that the jump length and frequency for the unaged nano-silica/PDMS system gradually decrease with an increase in the aging level of PDMS, whereas show an increasing tendency with temperature However, the results of average caging time (Fig. 12b) indicate that H_2O molecules devote most of time (90.8–96.5%) to the oscillating motions in the microcavities. The reasons for these phenomena are due to the dominant effects of the hydroxyl groups and cross-linking over the scission of the main chain. The formation of the stronger polar interactions and cross-linking reduces the local thermal motion of the PDMS chains and the FAV for movement, and thereby lowering the probability of the formation of the temporary channels between adjacent cavities available for H_2O molecules to jump. In addition, the hydroxyl groups can also form H-bonds with the hydroxyl groups of the PDMS chains (Fig. 10a), which also decreases the diffusion rate of H_2O molecules. H_2O molecules may jump from one polar site to another or into a neighboring cavity via a temporary channel formed by the thermal movement of the PDMS chains. Furthermore, the jump length and frequency of H_2O molecules for all systems increase with an increase in temperature (Fig. 11e, f), due to the increase in the mobility of PDMS chains and H_2O molecules as the temperature increases accompanied by the higher probability of the formation of the temporary channels.

During the radiation-moisture aging process, the moisture is not only involved in the aging-induced chemical reactions resulting in the degradation of the polymer matrix but also forms intermolecular interactions with the silica and PDMS chains containing polar groups. Meanwhile, the bonding strength of the silica-PDMS interface may deteriorate as moisture permeates into the interface. These behaviors have a significant effect on the thermal and mechanical properties of composites. Figure 13(a) shows the MSDs of the H_2O molecules near the silica and PDMS surfaces in the unaged and aged silica-PDMS interface systems. For all interface systems, it is seen that the MSD of H_2O molecules near the silica surface is larger than that near the PDMS surface, which means the lower diffusion mobility and rate of H_2O molecules near the PDMS surface. Furthermore, the MSDs of the H_2O molecules near the PDMS surface continuously increase with an increase in aging level, implying an increase in diffusion mobility and rate of H_2O molecules. There are two reasons for this phenomenon. First of all, the H_2O molecules can form H-bonds with the hydroxyl groups and oxygen of Si-O-Si on the surface of the silica and PDMS matrix, as shown in Fig. 14a. In addition, we observe that a single H_2O molecule can also form multi-H-bonds with the other polar groups on the surface of the silica and PDMS matrix. As the aging level increases, the formation of more hydroxyl groups on the surface of the aged PDMS means a higher probability to form more H-bonds with H_2O molecules compared with the unaged PDMS, which will restrict the movement of H_2O molecules. Thus, the PDMS and silica can adsorb many H_2O molecules on their surfaces leading to a high concentration of H_2O molecules, thereby slowing the diffusion rate of H_2O molecules. Secondly, some H_2O molecules diffuse into the PDMS matrix region by thermal movement, whereas the PDMS chains restrict H_2O molecules to get out during the simulation process. Meanwhile, the aged PDMS matrix restrains H_2O molecules to diffuse into the PDMS matrix surface region due to the denser PDMS matrix and strong intermolecular interactions between PDMS chains, which is in agreement with the results of MSD of H_2O molecules in the unaged and aged nano-silica/PDMS systems. Figure 13(b) shows the typical MSDs and diffusion trajectory of a single H_2O molecule along the Z-direction in the interface Model 1 and Model 4 systems. The results indicate that a single H_2O molecule makes continuous thermal movement between silica and PDMS matrix surfaces, and can pass through the PDMS matrix surface layer along with the formation of the temporary channels.

It should be noted from Fig. 14b that H_2O molecules can also form multi-H-bonds with the other H_2O molecules. This causes the agglomeration of several H_2O molecules leading to a further decrease in the diffusion mobility of H_2O molecules. Moreover, H_2O molecules can simultaneously form the H-bonds with the polar groups on the surface of the silica and PDMS matrix. This restricts the formation of stronger intermolecular interactions between the silica and PDMS matrix. In the previous section, we find that the severe aging of the PDMS matrix limits the H_2O

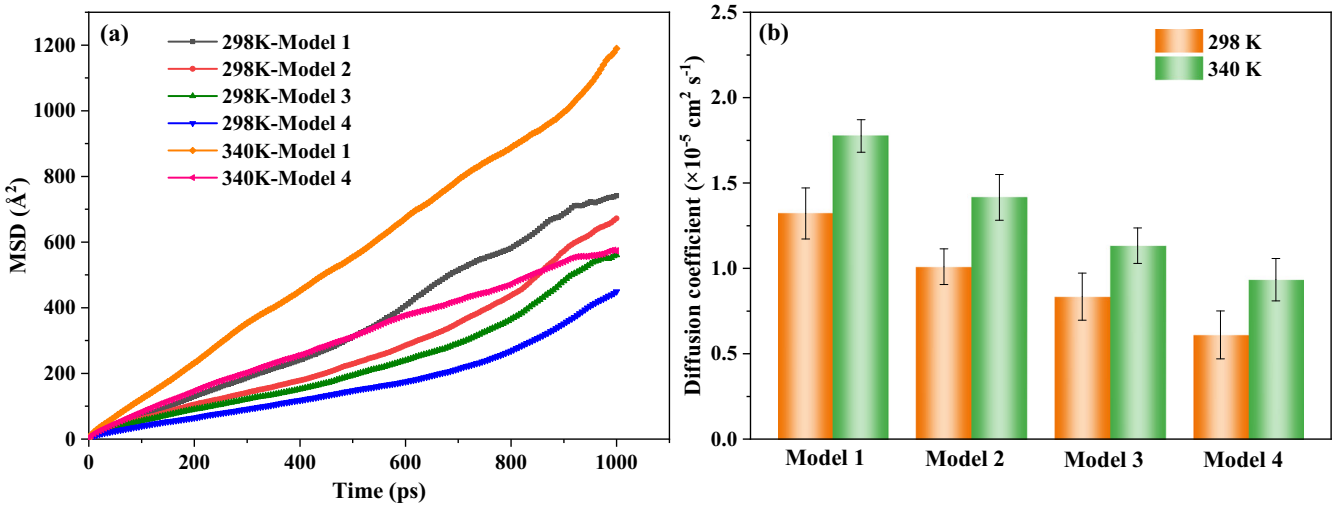

Fig. 9 Diffusion of H_2O molecules in the unaged and aged nano-silica/PDMS systems. a MSDs and **b** diffusion coefficients. The error bars stand for the standard deviations from five independent sample.

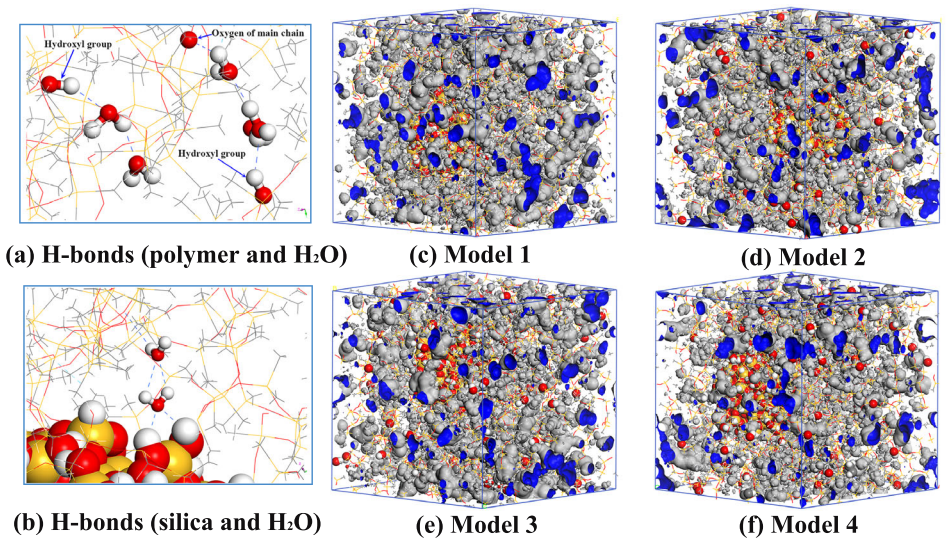

Fig. 10 The H-bonds and accessible volume for H_2O molecules in the unaged and aged nano-silica/PDMS systems. a H-bonds between the polymer chains and H_2O, **b** H-bonds between the silica and H_2O, **c** accessible volume in Model 1, **d** accessible volume in Model 2, **e** accessible volume in Model 3, and **f** accessible volume in Model 4.

molecules to permeate into the PDMS matrix surface layer. These phenomena will cause more H_2O molecules to aggregate in the silica-PDMS interface, which inhibits the formation of strong intermolecular interactions, especially for the H-bonds between the silica and PDMS matrix. This will somewhat weaken the binding strength between the silica and PDMS matrix. The deterioration of the bonding strength of the silica-PDMS interface will further degrade the physical and mechanical properties of the silicone rubber composites.

METHODS

Molecular models

The chemical processes of PDMS-based composites exposed to radiation-moisture environments primarily involve chain scission, cross-linking, breakage of side groups, formation of hydroxyl groups and gas products, and surface changes of silica filler during the long-term aging process. Generally, chain scission and cross-linking reactions occur simultaneously, and cross-linking reactions dominate over chain scission reactions during the aging process[5,7,27,53]. The typical cross-links include silethylene (Si-C-C-Si), silmethylene (Si-C-Si), silicon-oxygen-silicon (Si-O-Si), and silicon-silicon (Si-Si) links. Here, the formation of Si-C-C-Si cross-links originates from the combining of two methyl side groups radicals ($Si\text{-}CH_2\bullet$). Similarly, Si-C-Si cross-links are considered to form from the bonding between silicon-center radical (Si•) and $Si\text{-}CH_2\bullet$. The radiation-induced $Si\text{-}CH_2\bullet$ can be generated from the breakage of methyl side groups ($Si\text{-}CH_3 \rightarrow Si\text{-}CH_2\bullet + \bullet H$). The radiation-induced Si• can arise from the breakage of methyl side groups ($Si\text{-}CH_3 \rightarrow Si\bullet + \bullet CH_3$) and scission of the main chain ($Si\text{-}O\text{-}Si \rightarrow Si\text{-}O\bullet + Si\bullet$), accompanied by the formation of hydrogen (H_2) methane (CH_4), and ethane (C_2H_6). In addition, the joining of two Si• produces Si-Si cross-links. On the other hand, H• and •OH can be generated from the radiolysis of H_2O under the effect of radiation. The free radicals ($Si\text{-}CH_2\bullet$ and Si•) can react with H• and •OH to produce $Si\text{-}CH_2\text{-}OH$ and Si-OH. The silanol groups further combine stoichiometrically to make Si-O-Si cross-links.

To investigate the influence of radiation and moisture-induced chemical changes on thermodynamic and interface properties of

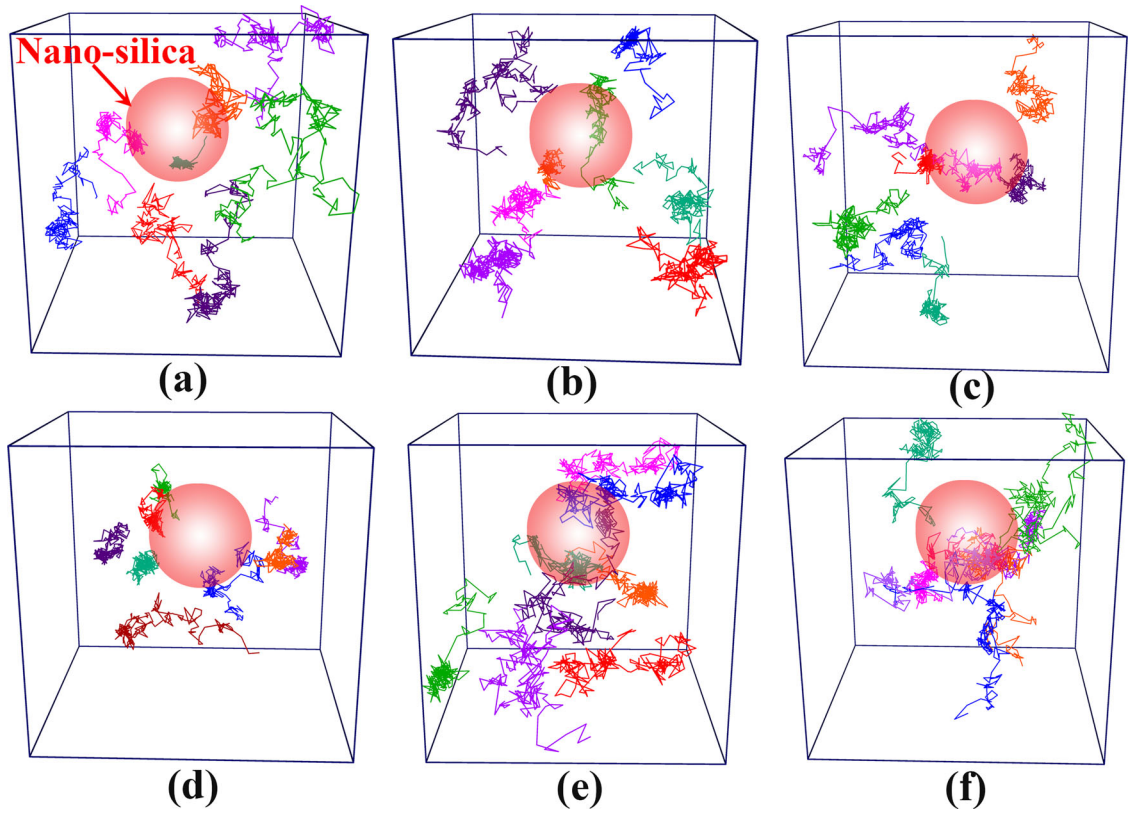

Fig. 11 The diffusion trajectories of H_2O molecules in the unaged and aged nano-silica/PDMS models at different temperatures. a Model 1 at 298 K, **b** Model 2 at 298 K, **c** Model 3 at 298 K, **d** Model 4 at 298 K, **e** Model 1 at 340 K, and **f** Model 4 at 340 K.

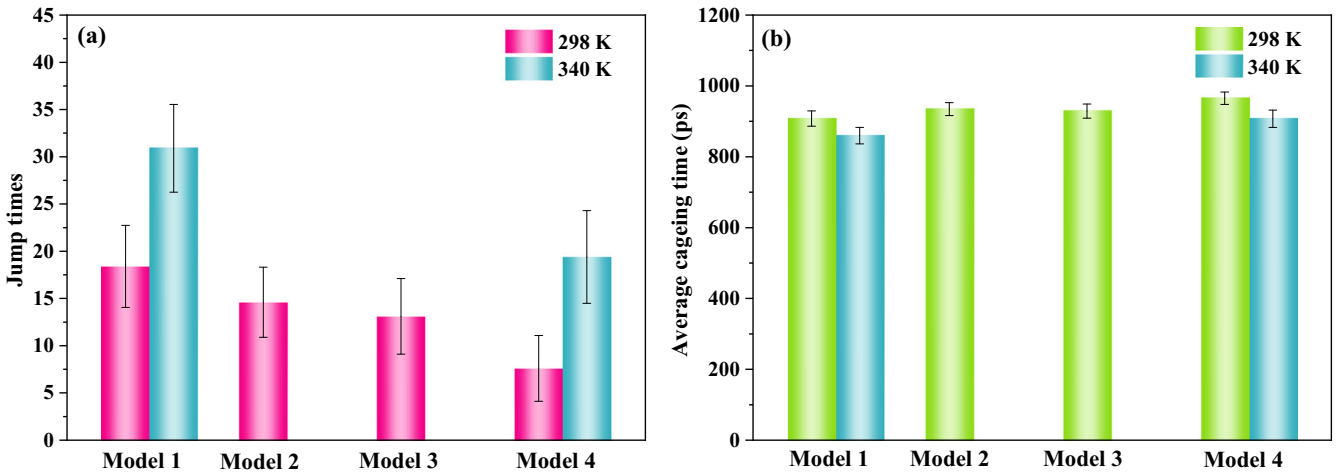

Fig. 12 Jump of H_2O molecules in different nano-silica/PDMS models at 298 K and 340 K. a Jump times and **b** average cageing time. The error bars stand for the standard deviations from five independent sample.

nano-silica/PDMS composites, the unaged and aged nano-silica/PDMS model, nano-silica/H_2O/PDMS model, PDMS-silica interface model, and PDMS-H_2O-silica interface model were constructed using Accelrys Materials Studio software by incorporating the hydrolysis products, cross-linking, and chain scission of PDMS matrix. The constructed unaged and aged PDMS chains are shown in Fig. 15. Figure 15a shows the typical molecular structure and repeat unit of PDMS. The initially constructed terminal hydroxyl group of the PDMS chain (chain A) with 30 repeat units is shown in Fig. 15b. The aging-induced crosslinking structures (Fig. 15c, chain B, and Fig. 15d, chain C) are formed via the joining of two chains. Four hydroxyl groups induced by hydrolysis also exist in chains B and C. The scission of the Si-O-Si main chain forms two unstable short chains, which can react with H_2O to generate stable short chains including hydroxyl groups (Fig. 15e, chain D_1 and D_2) or further combine with other chains to form new cross-links (Fig. 15f, chain E). Figure 15g shows a three-chain cross-linking structure (chain E) with one Si-C-Si cross-link, one Si-C-C-Si cross-link, and six hydroxyl groups. A four-chain cross-linking structure (chain G) was also constructed via two Si-C-Si cross-links, one Si-C-

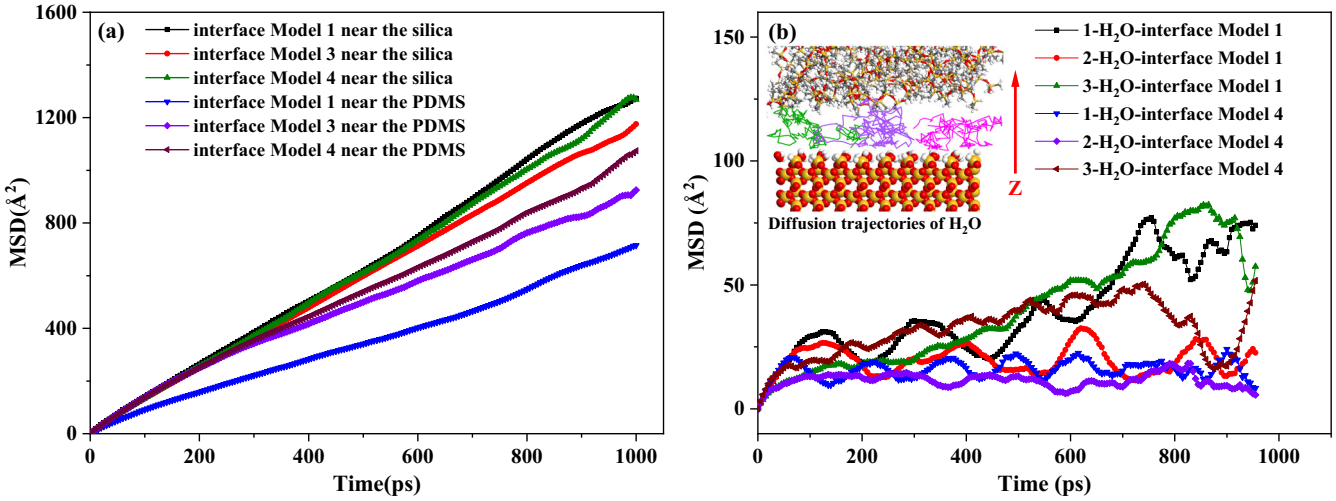

Fig. 13 MSDs of H_2O molecules in the different silica-PDMS interfaces. a Near the silica and PDMS, and **b** along the Z-direction.

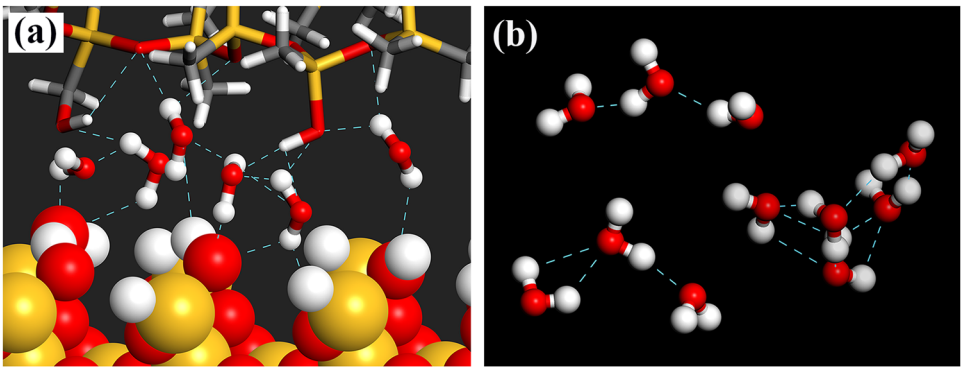

Fig. 14 H-bonds between H_2O molecules and other polar groups. a Polar groups on the surface of the silica and PDMS matrix, and **b** hydroxyl groups of H_2O molecules.

C-Si cross-link, and eight hydroxyl groups, as shown in Fig. 15h. In addition, a nano-silica particle with a diameter of 12 Å was constructed, as shown in Fig. 16a. The surface of nano-silica was modified using hydroxyl groups based on the experiment observation[8]. A surface of silica in contact with the PDMS matrix was cleaved along (0 0 1) crystallographic orientation of quartz lattice with a thickness of 10.8 Å[19]. A three-dimensional silica layer with a lattice parameter of 49.13 Å (X) × 49.13 Å (Y) × 10.8 Å (Z) was built, and then the surface was modified via hydroxyl groups, as shown in Fig. 16b).

All initially constructed PDMS chains underwent geometry optimization before further construction into composite systems. The unaged and aged nano-silica/PDMS and PDMS-silica interface models were constructed using the optimized PDMS chains, nano-silica particle, and silica layer. Besides, by regulating the composition ratios of the unaged and aged PDMS chains, the unaged, short-term aged, medium-term aged, and long-term aged nano-silica/PDMS and PDMS-silica interface model systems were constructed based on the dominant role of the cross-linking over chain scission, respectively. The composition ratios of each component in the unaged and aged models are shown in Table 1. For each nano-silica/PDMS and PDMS-silica interface configurations, a total number of five parallel models with the same composition were randomly generated to obtain reliable simulation results. The PDMS layers of interface model 1-4 have a thickness of 34.98 Å, 35.10 Å, 35.26 Å, and 35.24 Å, respectively. The supercell size of these PDMS layers in the X and Y directions is 44.21 Å × 44.21 Å. To investigate the effect of radiation-moisture aging on the H_2O diffusion in the nano-silica/PDMS and silica/PDMS interface, 16 H_2O molecules were added in the unaged and aged nano-silica/PDMS (Fig. 16c) model systems to construct the nano-silica/H_2O/PDMS models (Fig. 16d), and an H_2O layer with a thickness of 6 Å was added in the interface (Fig. 16e) to build the PDMS-H_2O-silica interface model (Fig. 16f). Additionally, a 60 Å vacuum layer was set on top of the PDMS layer to avoid probable interactions with the upper silica layer.

It is worth noting that the thermodynamic properties (such as glass transition temperature and diffusion coefficients) of nano-silica/PDMS composites depends on interfacial interaction, cross-linking density, chain rigidity, chain aggregation, chain confinement, process conditions, volume fraction of additives, etc[5,54]. The variations of these factors can alter the final thermodynamic properties, and this study focuses on the joint impact of hydrolysis products, chain scission, and cross-linking on the thermodynamic properties of nano-silica/PDMS composites. The decorrelated influence of each of the individual factors on thermodynamic properties requires a new simulation setup via the factor-control design of experiment method and ReaxFF software, and this part will be studied in the future.

MD simulation methods

In this work, the MD simulations were performed using the Materials Studio software. The classical COMPASS (condensed-

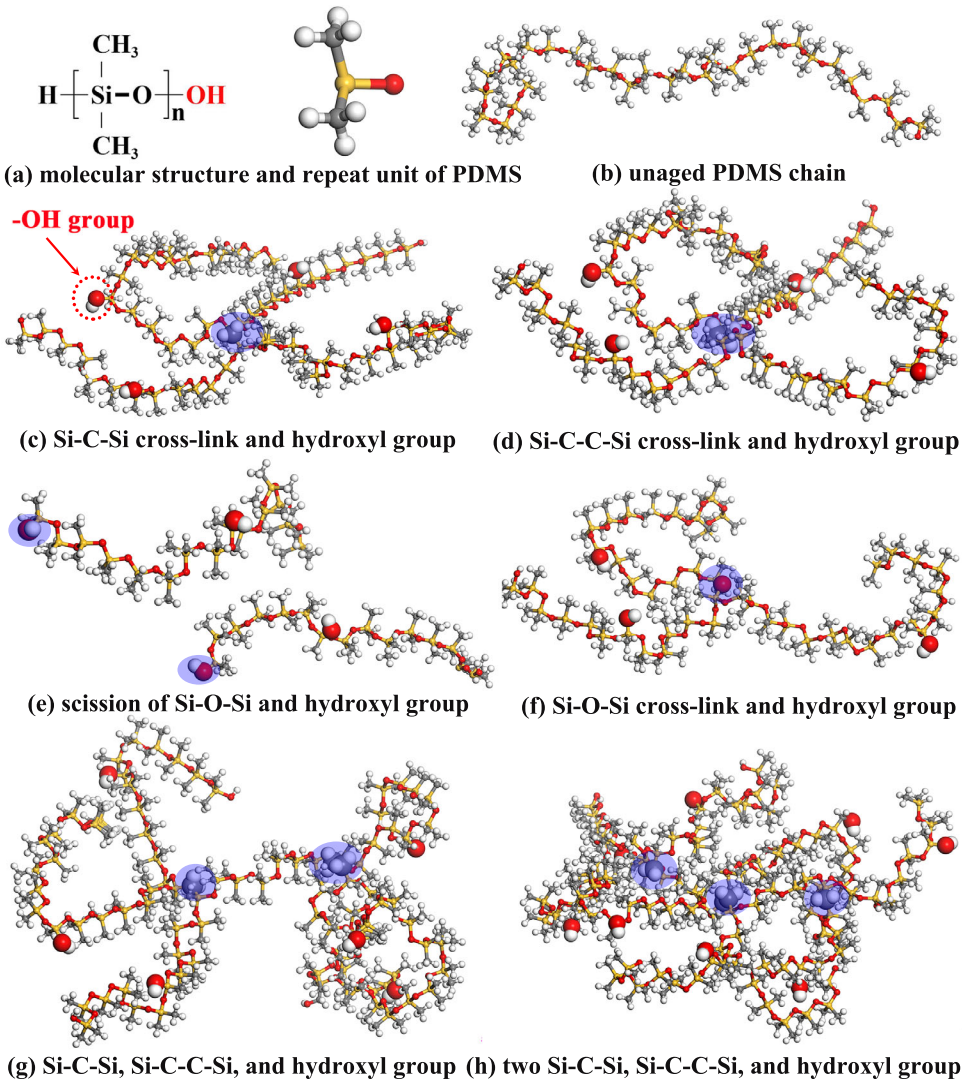

Fig. 15 The chemical structures of the unaged and aged PDMS chains. a Molecular structure and repeat unit of PDMS, (**b**) unaged PDMS chain (A), (**c**) aged chain B with one Si-C-Si cross-link and four hydroxyl groups, (**d**) aged chain C with one Si-C-C-Si cross-link and four hydroxyl groups, (**e**) scission chain D_1 and D_2 of Si-O-Si main chain with two hydroxyl groups, (**f**) cross-linking structure (E) after scission chain with three hydroxyl groups, (**g**) cross-linking structure (F) with one Si-C-Si cross-link, one Si-C-C-Si cross-link, and six hydroxyl groups, and (**h**) cross-linking structure (G) with two Si-C-Si cross-links, one Si-C-C-Si cross-link, and eight hydroxyl groups.

phase optimized molecule potentials for atomistic simulation studies) force field was used to describe molecule interactions in nano-silica/PDMS and PDMS-silica interface model systems[55]. This force field is widely suitable for most common organics, small inorganic molecules, and polymers, and can accurately predict the structural and thermophysical condensed phase properties of the related materials under a wide range of temperature and pressure conditions. However, to the best of the authors' knowledge, available reactive force field tools cannot directly simulate the radiation-moisture aging-induced chemical changes. Therefore, an alternative route is taken to investigate the effect of radiation-moisture aging on the thermodynamic and interface properties by constructing a series of PDMS systems that incorporate the hydrolysis products, cross-linking, and chain scission of the PDMS matrix. In all simulations, the Andersen thermostat and Berendsen barostat were utilized to control the temperature and pressure for all NVT (constant number of particles, volume, and temperature) and NPT ensembles with a time step of 1 fs, respectively[56–58]. The non-bonded interactions were calculated by the atom-based method and the Ewald method. During a simulation process, geometry optimization with an energy convergence tolerance of 1.0×10^{-5} kcal mol^{-1} and force convergence tolerance of 5×10^{-3} kcal mol^{-1} Å^{-1} was first conducted to obtain a state of minimum potential energy for each model using the Smart Minimizer method. Subsequently, fifty annealing cycles with five heating ramps per cycle were performed under the temperature ranged from 300 to 600 K. Then, these systems were subjected to 500 ps of NVT ensemble at 298 K and 500 ps of NPT ensemble at 298 K and 1 atm to continuously relax these systems. Finally, a 1000 ps of NPT ensemble at 298 K and 1 atm was conducted to achieve the stable system configuration. After that, the simulated densities of the nano-silica/PDMS models were obtained during the final 1000 ps NPT simulation, as shown in Fig. 17. A relatively stable density with a small deviation (≤2%) can be observed for each model, which indicates that each system achieved an equilibrium state. The molecular trajectories were used to analyze the changes in the microstructure, thermodynamics, and interface properties of systems.

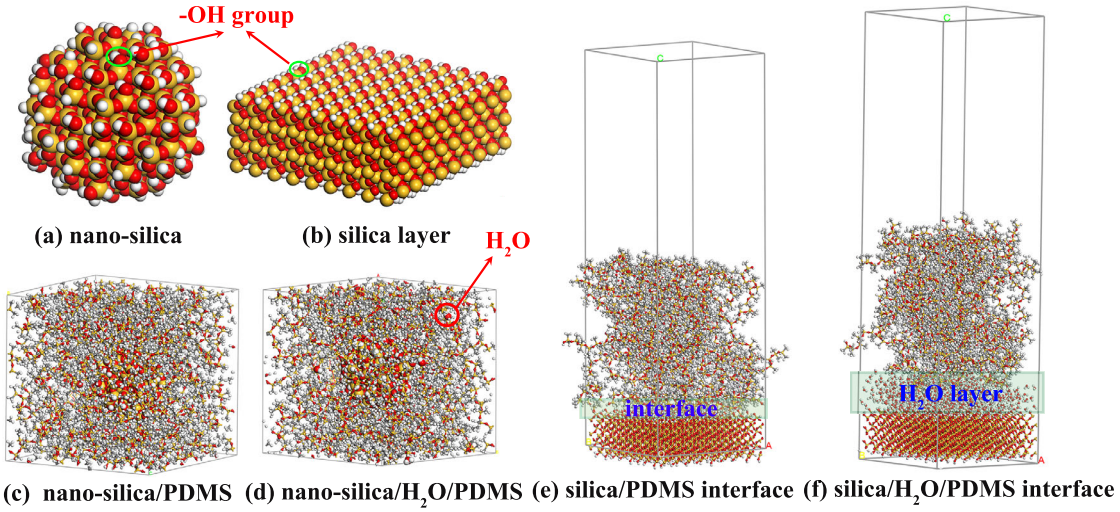

Fig. 16 Construction of nano-silica/PDMS and PDMS-silica interface models. a Molecular structure of nano-silica, **b** molecular structure of silica layer, **c** nano-silica/PDMS composite, **d** nano-silica/H_2O/PDMS, **e** silica/PDMS interface, and **f** silica/H_2O/PDMS interface.

Table 1. Constructions of the unaged and aged molecular models.

Molecular model	No. of chains								No. of nano-silica	No. of silica layer
	A	B	C	D_1	D_2	E	F	G		
Model 1	32								1	
Model 2	10	4	4	2	4	3			1	
Model 3		6	3	4	3	10			1	
Model 4				2	2	4	4	3	1	
Interface model 1	32									1
Interface model 2	10	4	4	2	4	3				1
Interface model 3		6	3	4	3	10				1
Interface model 4				2	2	4	4	3		1

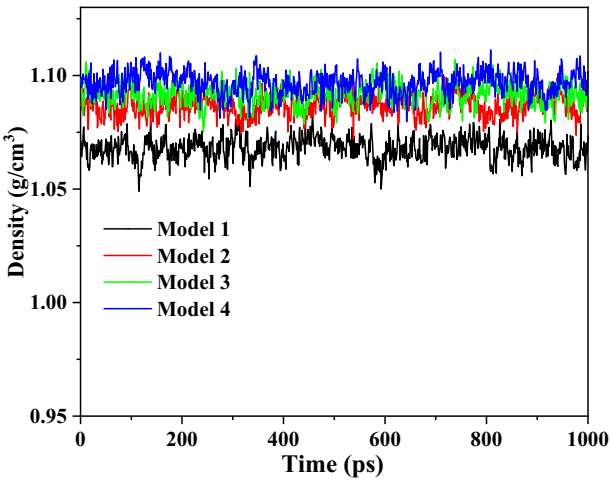

Fig. 17 Simulated density of the nano-silica/PDMS models as a function of simulation time.

DATA AVAILABILITY

The data that support the findings of this study are available from the corresponding author upon reasonable request.

Received: 6 January 2023; Accepted: 31 March 2023;
Published online: 19 April 2023

REFERENCES

1. Maxwell, R. S., Cohenour, R., Sung, W., Solyom, D. & Patel, M. The effects of γ-radiation on the thermal, mechanical, and segmental dynamics of a silica filled, room temperature vulcanized polysiloxane rubber. *Polym. Degrad. Stabil.* **80**, 443–450 (2003).
2. Roggero, A. et al. Inorganic fillers influence on the radiation-induced ageing of a space-used silicone elastomer. *Polym. Degrad. Stabil.* **128**, 126–133 (2016).
3. Kaneko, T., Ito, S., Minakawa, T., Hirai, N. & Ohki, Y. Degradation mechanisms of silicone rubber under different aging conditions. *Polym. Degrad. Stabil.* **168**, 108936 (2019).
4. Fang, H. et al. Radiation induced degradation of silica reinforced silicone foam: Experiments and modeling. *Mech. Mater.* **105**, 148–156 (2017).
5. Celina, M., Linde, E., Brunson, D., Quintana, A. & Giron, N. Overview of accelerated aging and polymer degradation kinetics for combined radiation-thermal environments. *Polym. Degrad. Stabil.* **166**, 353–378 (2019).
6. Lou, W., Xie, C. & Guan, X. Coupled effects of temperature and compressive strain on aging of silicone rubber foam. *Polym. Degrad. Stabil.* **195**, 109810 (2022).
7. Wang, P. C. et al. Coupling effects of gamma irradiation and absorbed moisture on silicone foam. *Mater. Des.* **195**, 108998 (2020).
8. Yan, S. et al. Influence of γ-irradiation on mechanical behaviors of poly methyl-vinyl silicone rubber foams at different temperatures. *Mech. Mater.* **151**, 103639 (2020).
9. Liu, B. et al. Effects of combined neutron and gamma irradiation upon silicone foam. *Radiat. Phys. Chem.* **133**, 31–36 (2017).
10. Patel, M. et al. Complexities associated with moisture in foamed polysiloxane composites. *Polym. Degrad. Stabil.* **93**, 513–519 (2008).
11. Maiti, A., Gee, R. H., Weisgraber, T., Chinn, S. & Maxwell, R. S. Constitutive modeling of radiation effects on the permanent set in a silicone elastomer. *Polym. Degrad. Stabil.* **93**, 2226–2229 (2008).
12. Jia, D. et al. Constitutive modeling of γ-irradiated silicone rubber foams under compression and shear loading. *Polym. Degrad. Stabil.* **183**, 109410 (2021).
13. Zhu, L. et al. Tetraphenylphenyl-modified damping additives for silicone rubber: Experimental and molecular simulation investigation. *Mater. Des.* **202**, 109551 (2021).
14. Hill, D. J. T., Preston, C. M. L., Salisbury, D. J. & Whittaker, A. K. Molecular weight changes and scission and crosslinking in poly(dimethyl siloxane) on gamma radiolysis. *Radiat. Phys. Chem.* **62**, 11–17 (2001).
15. Wu, J., Niu, K., Su, B. & Wang, Y. Effect of combined UV thermal and hydrolytic aging on micro-contact properties of silicone elastomer. *Polym. Degrad. Stabil.* **151**, 126–135 (2018).
16. Loganathan, N., Muniraj, C. & Chandrasekar, S. Tracking and erosion resistance performance investigation on nano-sized SiO2 filled silicone rubber for outdoor insulation applications. *IEEE. Trans. Dielectr. El.* **21**, 2172–2180 (2014).

17. Sheng, K. et al. Increasing the surface hydrophobicity of silicone rubber by electron beam irradiation in the presence of a glycerol layer. *Appl. Surf. Sci.* **591**, 153097 (2022).
18. Jiang, B., Guo, H., Chen, D. & Zhou, M. Microscale investigation on the wettability and bonding mechanism of oxygen plasma-treated PDMS microfluidic chip. *Appl. Surf. Sci.* **574**, 151704 (2022).
19. Li, W. et al. The effects of interfacial water and SiO_2 surface wettability on the adhesion properties of SiO2 in epoxy nanocomposites. *Appl. Surf. Sci.* **502**, 144151 (2020).
20. Ghosh, D. & Khastgir, D. Degradation and stability of polymeric high-voltage insulators and prediction of their service life through environmental and accelerated aging processes. *ACS omega* **3**, 11317–11330 (2018).
21. Bleszynski, M. & Kumosa, M. Aging resistant TiO2/silicone rubber composites. *Compos. Sci. Technol.* **164**, 74–81 (2018).
22. Wu, J., Dong, J., Wang, Y. & Gond, B. K. Thermal oxidation ageing effects on silicone rubber sealing performance. *Polym. Degrad. Stabil.* **135**, 43–53 (2017).
23. Gillen, K. T. & Kudoh, H. Synergism of radiation and temperature in the degradation of a silicone elastomer. *Polym. Degrad. Stabil.* **181**, 109334 (2020).
24. Tan, J. Z., Chao, Y. J., Li, X. D. & Van, J. W. Degradation of silicone rubber under compression in a simulated PEM fuel cell environment. *J. Power Sources* **172**, 782–789 (2014).
25. Maiti, A., Small, W., Lewicki, J. P., Chinn, S. C. & Saab, A. P. Age-aware constitutive materials model for a 3d printed polymeric foam. *Sci. Rep.* **9**, 15923 (2019).
26. Maiti, A. et al. Thermal aging of traditional and additively manufactured foams: analysis by time-temperature-superposition, constitutive, and finite-element models. (Lawrence Livermore National Lab., Livermore, United States, 2016).
27. Qin, Z. M., Wang, P. C. & Chen, H. B. Coupling effects of gamma irradiation and moisture on the properties of SiO2 and TiO2 filled silicone rubber. *Radiat. Phys. Chem.* **197**, 110190 (2022).
28. Maiti, A. et al. Constitutive model of radiation aging effects in filled silicone elastomers under strain. *J. Phys. Chem. B.* **125**, 10047–10057 (2021).
29. Wang, H. Y., Qiu, Y., Hu, W. J. & Chen, Y. M. Gamma radiation induced compressive response of silicon rubber foam: Experiments and modeling. *J. Mater. Res.* **34**, 2914–2200 (2019).
30. Bleszynski, M. & Kumosa, M. Silicone rubber aging in electrolyzed aqueous salt environments. *Polym. Degrad. Stabil.* **146**, 61–68 (2017).
31. Luo, Y. et al. Temperature dependence of the interfacial bonding characteristics of silica/styrene butadiene rubber composites: a molecular dynamics simulation study. *RSC Adv.* **9**, 40062–40071 (2019).
32. Luo, K. et al. Synergistic effects of antioxidant and silica on enhancing thermo-oxidative resistance of natural rubber: Insights from experiments and molecular simulations. *Mater. Des.* **181**, 107944 (2019).
33. Bahlakeh, G. & Ramezanzadeh, B. A detailed molecular dynamics simulation and experimental investigation on the interfacial bonding mechanism of an epoxy adhesive on carbon steel sheets decorated with a novel cerium-lanthanum nanofilm. *ACS Appl. Mater. Interfaces* **9**, 17536–17551 (2017).
34. Wang, Z. et al. Effect of interfacial bonding on interphase properties in SiO2/epoxy nanocomposite: a molecular dynamics simulation study. *ACS Appl. Mater. Interfaces* **8**, 7499–7508 (2016).
35. Kroonblawd, M. P., Goldman, N., Maiti, A. & Lewicki, J. P. Polymer degradation through chemical change: a quantum-based test of inferred reactions in irradiated polydimethylsiloxane. *Phys. Chem. Chem. Phys.* **24**, 8142–8157 (2022).
36. Kroonblawd, M. P., Goldman, N., Maiti, A. & Lewicki, J. P. A quantum-based approach to predict primary radiation damage in polymeric networks. *J. Chem. Theory Comput.* **17**, 463–473 (2020).
37. Liu, Q. et al. Gamma Radiation Chemistry of Polydimethylsiloxane Foam in Radiation-Thermal Environments: Experiments and Simulations. *ACS Appl. Mater. Interfaces* **13**, 41287–41302 (2021).
38. Itsumi, K., Hosono, Y., Yamamoto, N. & Yamashita, Y. Low acoustic attenuation silicone rubber lens for medical ultrasonic array probe. *IEEE T. Ultrason. Ferr.* **56**, 870–874 (2009).
39. Yan, Y. et al. Molecular dynamics simulation of the interface properties of continuous carbon fiber/polyimide composites. *Appl. Surf. Sci.* **563**, 150370 (2021).
40. Brown, I. D. On the geometry of O–H··· O hydrogen bonds. *Acta Crystallogr. A.* **32**, 24–31 (1976).
41. Katrusiak, A. Stereochemistry and transformation of-OH… O= hydrogen bonds Part I. Polymorphism and phase transition of 1, 3-cyclohexanedione crystals. *J. Mol. Struct.* **269**, 329–354 (1992).
42. Chang, K. S. et al. Free volume and alcohol transport properties of PDMS membranes: Insights of nano-structure and interfacial affinity from molecular modeling. *J. Membr. Sci.* **417**, 119–130 (2012). ().
43. Shan, H. et al. Molecular dynamics simulation and preparation of vinyl modified polydimethylsiloxane membrane for pervaporation recovery of furfural. *Sep. Purif. Technol.* **258**, 118006 (2021).
44. Badenhoop, J. K. & Weinhold, F. Natural steric analysis: Ab initio van der Waals radii of atoms and ions. *J. Chem. Phys.* **107**, 5422–5432 (1997).
45. Dutta, R. C. & Bhatia, S. K. Structure and gas transport at the polymer-zeolite interface: insights from molecular dynamics simulations. *ACS Appl. Mater. Interfaces* **10**, 5992–6005 (2018).
46. Martı, J. Analysis of the hydrogen bonding and vibrational spectra of supercritical model water by molecular dynamics simulations. *J. Chem. Phys.* **110**, 6876–6886 (1999).
47. Ahmad, A., Li, S. H. & Zhao, Z. P. Insight of organic molecule dissolution and diffusion in cross-linked polydimethylsiloxane using molecular simulation. *J. Membr. Sci.* **620**, 118863 (2021).
48. Tamai, Y., Tanaka, H. & Nakanishi, K. Molecular simulation of permeation of small penetrants through membranes. 1. *Diffus. Coeff. Macromolecules.* **27**, 4498–4508 (1994).
49. Wei, Q., Zhang, Y., Wang, Y., Chai, W. & Yang, M. Measurement and modeling of the effect of composition ratios on the properties of poly (vinyl alcohol)/poly (vinyl pyrrolidone) membranes. *Mater. Des.* **103**, 249–258 (2016).
50. Li, W., Zhang, L., Zhang, M. & Chen, S. Structures of graphene-reinforced epoxy coatings and the dynamic diffusion of guest water: a molecular dynamics study. *Ind. Eng. Chem. Res.* **59**, 20749–20756 (2020).
51. Müller-Plathe, F. Diffusion of water in swollen poly (vinyl alcohol) membranes studied by molecular dynamics simulation. *J. Membr. Sci.* **141**, 147–154 (1998).
52. Chen, Z., Gu, Q., Zou, H., Zhao, T. & Wang, H. Molecular dynamics simulation of water diffusion inside an amorphous polyacrylate latex film. *J. Polym. Sci. Poly. Phys.* **45**, 884–891 (2007).
53. Lou, W., Xie, C. & Guan, X. Thermal-aging constitutive model for a silicone rubber foam under compression. *Polym. Degrad. Stabil.* **198**, 109873 (2022).
54. Guo, G. et al. Molecular-dynamics study on the thermodynamic properties of nano-SiO2 particle-doped silicone rubber composites. *Comp. Mater. Sci.* **212**, 111571 (2022).
55. Zhu, L. et al. Effects of chain structure on damping property and local dynamics of phenyl silicone rubber: Insights from experiment and molecular simulation. *Polym. Test.* **93**, 106885 (2021).
56. Koopman, E. A. & Lowe, C. P. Advantages of a Lower-Andersen thermostat in molecule dynamics simulations. *J. Chem. Phys.* **124**, 137 (2006).
57. Davoodi, J. & Ahmadi, M. Molecule dynamics simulation of elastic properties of CuPd nanowire. *Compos. Part B-Eng.* **43**, 10 (2012).
58. Lou, W., Xie, C. & Guan, X. Understanding radiation-thermal aging of polydimethylsiloxane rubber through molecular dynamics simulation. *npj Mater. Degrad.* **6**, 84 (2022).

ACKNOWLEDGEMENTS

This work was supported by National Natural Science Foundation of China, Nos. U2230204, 12088101, and CAEP CX20200035. The support is gratefully acknowledged.

AUTHOR CONTRIBUTIONS

W.L.: Methodology, Writing-Original Draft Preparation. C.X.: Methodology. X.G.: Writing—review & editing.

COMPETING INTERESTS

The authors declare no competing interests.

ADDITIONAL INFORMATION

Correspondence and requests for materials should be addressed to Chaoyang Xie or Xuefei Guan.